# Energy Efficiency in Aquaculture: Outperforming Rule-Based HVAC Control with Nonlinear MPC

Klaas Völtzer, Jonathan Klinge, Axel Hackbarth

Abstract—
Humidity control in indoor recirculating aquaculture systems (RAS) is critical to prevent mold and structural damage, but remains highly energy-intensive due to constant evaporation from open water bodies. Although Model Predictive Control (MPC) is established in building automation, few studies address the complex hygrothermal dynamics specific to aquaculture environments. This paper presents a model-in-the-loop evaluation of a nonlinear MPC designed for an aquaculture hall in Northern Germany, using a gray-box RC model adapted via an Extended Kalman Filter. Simulations conducted over a one-year period compare the MPC against an advanced rule-based baseline controller, focusing on the impact of prediction horizons and mode switching strategies. The results demonstrate that the nonlinear MPC consistently outperforms the baseline, achieving energy savings between 12.1 % and 18.5 %. The highest efficiency was achieved using a 24-hour blocked prediction horizon with cost-optimal mode switching. Furthermore, the controller showed significant robustness, maintaining 13.1 % savings even when subjected to a 10 % model parameter mismatch. These findings confirm the potential of nonlinear MPC to optimize energy consumption in complex, humidity-critical industrial facilities.

## I. Introduction

Heating, ventilation, and air conditioning (HVAC) account for 60 % of the energy consumed in European buildings [1] and around 10 % to 20 % of the total energy demand in developed countries [2]. In 2024, the EU revised its directive "on the energy performance of buildings," assigning a key role to building automation and control systems, as well as other "smart" solutions, in implementing the "Energy Efficiency First" principle [3]. The use of optimal control in buildings, specifically model predictive control (MPC), has been thoroughly studied within the scientific community [4, 5], but only a few have investigated hygrothermal building models for MPC in simulations [6, 7, 8, 9] or in real-life over a short time frame of several days [10]. Swimming pools, agricultural buildings and indoor aquaculture have a dominant humidity and evaporation dynamic that need to be modeled accordingly [11]. De-humidification with HVAC systems is required to prevent mold and comply with local workplace regulations.

A problem in the real-life application of MPC in buildings is that in contrast to simulations or rather unvarying processes in industry plants, buildings are subject to change. Internal loads and model parameters may unexpectedly vary due to changes in the building itself or changes in the environment. [12, 13] were the first to propose the use of an Extended Kalman Filter (EKF) for adaptive building modeling to cope with a changing system. The hall investigated in this case study incorporates indoor recirculating aquaculture systems (RAS), allowing a sustainable operation of fish production in an enclosed environment. Due to the high humidity in indoor aquaculture, high air exchange rates (or artificial dehumidification) are necessary to keep humidity in an acceptable range to prevent the growth of fungi and/or corrosion. A significant potential for energy savings was identified in the switch to a dynamic facility ventilation [14]. A model for a different HVAC system in the same investigated facility has already been analyzed in [15] and was adapted in this paper. This research focuses on the control of an HVAC-system model, aiming to keep indoor temperature and humidity within acceptable bounds and to prevent condensation while minimizing energy consumption. The approach is validated in a software-in-the-loop environment with model mismatch. The advantage of the MPC, which acts directly on the low-level inputs of the HVAC unit, is demonstrated in comparison with a state-of-the-art rule-based PID controller.

## II. Method

This section presents the methods used to assess MPC performance. Firstly, we summarize the case study building and its modeling which is described in a previous publication [15]. We then present the control baseline used for comparison and provide a description of the non-linear optimization problem for the MPC formulation. The last section outlines the factors investigated that affect MPC performance.

### A. Case Study Building

The case study building is located in Büsum, Germany and hosts a Fraunhofer IMTE research facility for RAS. The hall that is the object of this study has a volume of roughly $2500\,\mathrm{m}^3$ with an external surface area of approximately $700\,\mathrm{m}^2$ (see Figure 1). The external surface is divided into four sections: The roof $w_1$, the east wall $w_2$, the south wall $w_3$ and the west wall $w_4$. Translucent windows on the roof provide natural light. One full wall of the hall adjoins a neighboring hall, and part of another wall adjoins a small conference room. Within the hall lies a small utility room containing various technical equipment, including heating. The facility runs several RAS experimental setups, with fish species changing multiple times per year. Required water temperatures are 12 - 25 °C, partially with high

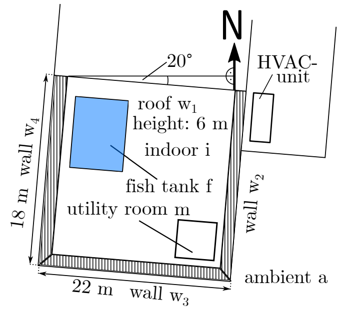


Fig. 1. Schematic of the aquaculture hall [15]

salinity. In hot periods hall temperatures exceed 30 ℃, overwhelming the existing water-cooling system. The current HVAC unit consists of a heat recovery unit and a heating coil, cannot meet the climate demand and will be replaced by an MPC-controlled system. The primary contributors to vapor loads include the bio-filter, exposed water tanks, aquariums and channels, cleaning activities, and personnel. Heat/cooling loads arise from technical equipment, temperature-controlled water, and occupants. Figure 2 shows the HVAC unit used in the

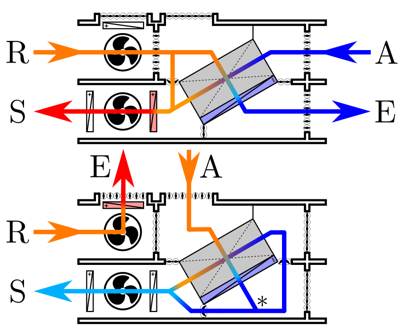


Fig. 2. Schematic of the planned HVAC unit in winter mode (top) and summer mode (bottom) with Ambient (A), Supply (S), Return (R) and Exhaust air (E)

indoor-climate simulation. The HVAC unit contains a heat recovery unit, a heat pump and a heating coil. Two configurations are considered: In winter mode, In winter mode the exhaust air may be recirculated and/or exchanged with ambient air via the heat-recovery unit; the heat pump transfers heat from exhaust to supply air. In summer mode, the heat pump transfers heat from the ambient air stream to the return/exhaust air stream. After passing through the heat recovery unit and the evaporator, the ambient air stream can be reheated by passing through the heat recovery unit again and/or directly enter the supply air stream via a bypass. The HVAC unit is expected to provide continuously adjustable flow rates between $1200\,\mathrm{m^3/h}$ and $6300\,\mathrm{m^3/h}$, continuously adjustable heat pump compressor power up to $5\,\mathrm{kW_{el}}$, and heating coil heating power of up to $30\,\mathrm{kW}$. To prevent external air from entering the hall, the supply flow rate $\dot{V}_s$ is usually set to $100\,\mathrm{m^3/h}$ higher than the return flow rate $\dot{V}_r$.

## B. Model

Control performance in MPC depends on the accuracy of the model and the accurate prediction of future disturbances. Model complexity is limited by the computational resources of the embedded hardware on which the MPC will be implemented. A gray box approach was chosen for modeling, which is described in more detail in a previous publication [15]. The modeling of the HVAC unit and the aquaculture hall is done separately, but both are combined into a single model. Before describing these two models, model foundations are described. Air density $\rho = 1.2\,\mathrm{kg\,m^{-3}}$, heat capacity $c_p = 1\,\mathrm{kJ\,kg^{-1}\,K^{-1}}$, and vaporization enthalpy $\Delta h_{vap} = 2454\,\mathrm{kJ\,kg^{-1}}$ are assumed constant. Humidity is measured as RH $\phi$ in %, which is defined by the ratio of water vapor partial pressure $p_v$ and saturation vapor pressure $p_{sat}$:

$$\phi = \frac{p_v}{p_{sat}} \tag{1}$$

For modeling, knowledge of specific humidity $x$ in $\mathrm{kg_{vapor}\,kg^{-1}_{dry\ air}}$ is required. Conversion is done by first computing $p_{sat}$ using empirical formulas recommended by the World Meteorological Organization [16, 17].

1) HVAC: As the time constants of the HVAC unit are much smaller than those of the building and also smaller than the sampling rate, a static model is used. Given the lack of available data on the planned HVAC unit (see Figure 2), it is described by a relatively simple physics and empiric based model that treats the air as a one-dimensional flow. Here we only want to outline the special assumptions that are important for the control.

When two unsaturated air streams are mixed, or a single unsaturated stream is cooled (negative $\dot{Q}$), the resultant air may reach its saturation limit of $\phi = 100\,\%$. Consequently, any additional water vapor will condense and latent heat must be considered. Here, first the temperature $T_1$ is calculated, neglecting condensation. And then from $T_1$ and the specific humidity $q_1$ the temperature accounting for condensation $T_2$ in ℃ can be calculated as

$$T_2 = T_1 + \frac{\Delta h_{vap}(q_1 - q_{sat})}{c_p} \tag{2}$$

with the enthalpy of vaporization $\Delta h_{vap}$ in $\mathrm{kJ\,kg^{-1}}$ (given $T_2 > T_1$). Specific saturation humidity $q_{sat}$ in kg/kg is a function of air temperature $T_2$ and air pressure $p$. For $T_2$ no analytic solution is available and it is not computationally efficient to solve $T_2$ numerically in MPC optimization. Therefore, a shallow feed-forward neural network is trained to estimate $T_2$ from $T_1$, $q_1$, and $p$. The neural network has two hidden layers with 7 and 5 neurons respectively. The prediction has a mean squared error (MSE) of approx. $3.1 \times 10^{-7}$ ℃.

The power of the heat pump can be continuously adjusted. In [18] the coefficient of performance (COP) for on-off modulating air source heat pumps is estimated based on temperature difference. For simplicity, it is assumed that this quadratic regression is still valid for the variable heat pump:

$$COP = (6.08 - 0.09\Delta T + 0.0005\Delta T^2)0.85 \tag{3}$$

$\Delta T = T_H - T_C$ is the (air) temperature difference between sink ($T_H$) and source ($T_C$) in $K$. In this paper $T_H$ is defined as the temperature before the condenser and $T_C$ as the temperature after the evaporator. The electrical power consumed by the heat pump compressor $P_{hp}$ and the heat flow in the condenser $\dot{Q}_c$ can be calculated with $\dot{Q}_e$ the heat flow from the evaporator in kW to:

$$P_{hp} = |\dot{Q}_e|/(COP - 1);\ \dot{Q}_c = P_{hp}\,COP \tag{4}$$

Hydraulic power is proportional to the cube of the volumetric flow rate $\dot{V}$ in $\mathrm{m^3\,s^{-1}}$. The electrical fan power ($\approx$ fan heat flow) $P_f$ in $\mathrm{kW_{el}}$ also depends on the overall efficiency $\eta_f$ of the fan and motor. Given the limited data available on the planned HVAC unit, the known relations from the current similar HVAC unit shown in [14] are used for both fans and independent of the airflow configuration:

$$P_f = \frac{1}{\eta_f} 0.3990\dot{V}^3 \tag{5}$$

$$\eta_f = -18.8055\dot{V}^2 + 74.4230\dot{V} \tag{6}$$

These relations were fitted for flow rates from $2700\,\mathrm{m^3/h}$ to $6300\,\mathrm{m^3/h}$. For this study they are assumed valid outside that range down to $1200\,\mathrm{m^3/h}$.

2) Hall: As in many other studies [19] a simple RC model is used to describe the building as a network of alternating resistors $R$ and capacitors $C$, analogous to an electric circuit. The structure of the hall model largely corresponds to the model described in [15], where we optimized the model complexity in an grey box approach. The air, building envelope and internal building mass have a thermal capacity. The amount of heat transfer between these capacities is proportional to the product of the temperature difference and the inverse of the connecting resistance. Non-linear heat transfer is neglected in this model. The RC model (see Figure 3)

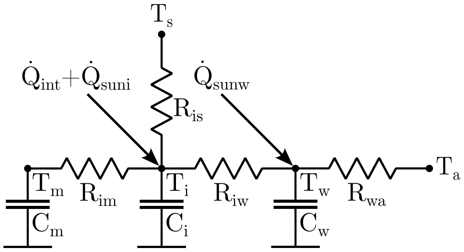


Fig. 3. Schematic of the hall RC model

can be described by the following equations:

$$\frac{C_i dT_i}{dt} = \dot{m}_s c_p (T_s - T_i) + \frac{T_w - T_i}{R_{iw}} + \frac{T_m - T_i}{R_{im}} + \dot{Q}_{int} + \dot{Q}_{suni} \tag{7}$$

$$\frac{C_w dT_w}{dt} = \frac{T_i - T_w}{R_{iw}} + \frac{T_a - T_w}{R_{wa}} + \dot{Q}_{sunw} \tag{8}$$

$$\frac{C_m dT_m}{dt} = \frac{T_i - T_m}{R_{im}} \tag{9}$$

Here, $T_i$ is the indoor temperature, which is equivalent to the return Temperature $T_r$ of the HVAC-unit (see Figure 3). $T_w$ is the temperature of the building envelope and $T_m$ is the temperature of the internal building mass like experimental setups and furniture. These three temperatures are modeled and have a corresponding capacity. Heat is exchanged between these capacities as well as with the supply air with temperature $T_s$ and ambient air with temperature $T_a$. The resistance between indoor air and supply air depends on the supply mass flow ($R_{is} = (\dot{m}_s c_p)^{-1}$). The resistance between the building envelope and ambient air is wind velocity dependent ($R_{wa} = (U_{wa} + c_w v_w)^{-1}$), where $U_{wa}$ is the thermal transmittance, $v_w$ is the wind velocity and $c_w$ is a coefficient for convective heat transfer. $\dot{Q}_{int}$ is the internal heat gain and $\dot{Q}_{suni} = A_{i1}\Phi_1 + A_{i4}\Phi_4$ is the direct solar heat gain with irradiance absorbing surfaces $A$ and solar irradiance $\Phi$ on the surfaces $w_1$ and $w_4$, where windows are located. The solar gain of the building envelope is a summation of the gains of all four sections of the external surface ($\dot{Q}_{sunw} = \sum_{w=1}^{4} A_w \Phi_w$).

The humidity inside the building is modeled by a single equation:

$$\frac{m_i dq_i}{dt} = \dot{m}_s(q_s - q_i) + \dot{q}_{evap} \tag{10}$$

Here, $q_i$ is the specific indoor humidity and $m_i$ is the indoor air mass. The change in humidity results from ventilation with specific supply humidity $q_s$ and evaporation $\dot{q}_{evap}$ in the hall. Evaporation from the open water surface is driven by the partial pressure gradient of vapor between the water surface. Only the indoor RH $\phi_i$ and the average indoor RH at wall temperature $\phi_{iw}$ are calculated (for details, see [15]). As the air mixture in the hall is not perfect, and the assumption of a constant envelope temperature is not true, humidity cannot be accurate simulated for a certain wall position.

3) HVAC + Hall: The hall model is discretized with the forward Euler method and, together with the HVAC-model, represented as a non-linear, discrete state space system with process noise $w_k$ and measurement noise $v_k$:

$$\hat{x}_{k+1} = f(\hat{x}_k, \hat{d}_k, u_k) + w_k \tag{11}$$

$$\hat{y}_k = h(\hat{x}_k, \hat{d}_k, u_k) + v_k \tag{12}$$

Model disturbances $\hat{d}$ are ambient temperature $T_a$, ambient specific humidity $\phi_a$, the surface dependent solar irradiance $\Phi_j$, wind velocity $v_w$, fish tank temperature $T_f$

and ambient air pressure $p$. Manipulated variables $u$ are the cooling power $\dot{Q}_e$ at the evaporator of the heat pump, the heating power of the heating coil $\dot{Q}_h$, volumetric flow rate of the supply air $\dot{V}_s$, air fraction $r \in [0, 1]$ and operational mode $m \in \{0, 1\}$ with $m = 1$ for winter mode and $m = 0$ for summer mode. The air fraction has a different meaning depending on the operational mode. In summer mode it is the fraction of $\dot{m}_a$ that passes through the heat recovery unit twice, and in winter mode it is the fraction of $\dot{m}_r$ that is recirculated into the supply air. Model outputs $y$ are indoor temperature $T_i$, indoor RH $\phi_i$, indoor RH at wall temperature $\phi_{iw}$, supply air temperature $T_s$, temperature at the heat pump evaporator $T_{ev}$, fan power consumption $P_f$ and heat pump power consumption $P_{hp}$. Model states are the temperatures of the internal building mass $T_m$, the envelope $T_w$ and the indoor air $T_i$ as well as the indoor specific humidity $q_i$.

All model parameters are kept constant except the irradiance absorbing surfaces $A$, the internal heat gain $\dot{Q}_{int}$, the evaporation coefficient $c_{evap}$ and the envelope capacity $C_w$. These parameters are estimated by the EKF to account for operational and seasonal changes, among others. The EKF also estimates the model states of the hall. The parameter sequence has been estimated using measured data and the model of the current HVAC unit described in [15]. Here, over the course of a year, the root mean squared error for a 24-hour ahead prediction is 0.45 °C for indoor temperature and 1.87 % for indoor humidity.

### C. Control

The control aims to keep indoor temperature and humidity within acceptable bounds and prevent condensation while minimizing energy use. Temperature limits follow the German workplace guidelines [20] at 17 °C and 26 °C for medium work intensity, with the lower limit reduced by 5 °C outside normal working hours on weekends and between 8 *pm* and 7 *am* on weekdays. Humidity is limited to 65 %. In high-humidity buildings the internal-wall-surface temperature must also be considered, and RH should not exceed 90 % to provide a safety margin. As our case study building lacks such a measurement, it is assumed that the envelope temperature of the hall model $T_w$ is that temperature. The HVAC supply air temperature $T_s$ is limited between 3 °C and 30 °C. Limits of the manipulated variables are displayed in Table I. The cooling power $\dot{Q}_e$ is only indirectly limited by the maximum power of the heat pump compressor $P_{hp}$ between 0 and 5 kW$_{\text{el}}$. For simplicity, it is assumed that the heat pump has no minimum power consumption. In the simulation $r$ is limited between 0.1 % and 99.9 % to avoid divisions by zero. Anti-icing protection is omitted.

TABLE I
List of manipulated variables with constraints

| index | description | min | max | unit |
|---|---|---|---|---|
| $u_1$ | $\dot{V}_s$ | 1300 | 6300 | m$^3$/h |
| $u_2$ | $r$ | 0 | 100 | % |
| $u_3$ | $\dot{Q}_h$ | 0 | 30 | kW |
| $u_4$ | $\dot{Q}_e$ | - | 0 | kW |
| $u_5$ | $m$ | 0 or 1 | | - |

1) Control baseline: To evaluate MPC performance a baseline control strategy is used. For each of the two HVAC modes, simple PI controllers and associated functions are employed. The overall sampling time is 1 min, except for inner cascades (10 sec). The design follows the same objectives as the MPC cost function: satisfy temperature and RH limits while minimizing energy demand. Lower-level controllers are excluded from the description as well as simulations. In winter

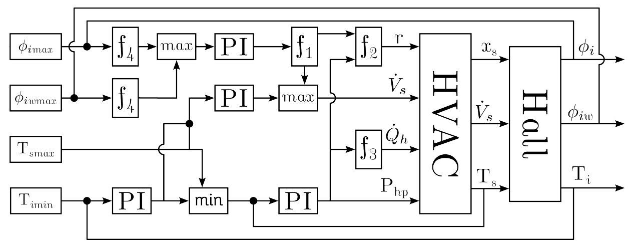


Fig. 4. Schematic of baseline control in winter mode

mode (see Figure 4) the indoor RH ($\phi_i$ and $\phi_{iw}$) is regulated by supplying drier outdoor air. RH violations are converted to specific-humidity errors ($f_4$); the larger error feeds a PI controller. The controller's output is converted by the function $f_1$ into HVAC inputs $r$ and $\dot{V}_s$. To increase the outdoor air exchange, at minimum supply flow rate, the recirculation $r$ is first reduced to its minimum before the volumetric supply flow rate $\dot{V}_s$ is increased. The indoor temperature $T_i$ is controlled in cascade with the supply air temperature $T_s$, whose setpoint is limited by $T_{smax}$. The output of the $T_s$ controller is the heat pump compressor power $P_{hp}$, which is the first choice for heating. To avoid insufficient mass flow at the evaporator, recirculation is disabled when the heat pump is in operation ($f_2$). When the heat pump reaches its limit, the surplus power is multiplied by 3 and applied as heating-coil power $\dot{Q}_h$ ($f_3$) to compensate for differing gains. If the set point for $T_s$ exceeds $T_{smax}$, a PI controller increases $\dot{V}_s$ to meet the heating demand without exceeding $T_{smax}$. In summer mode (see

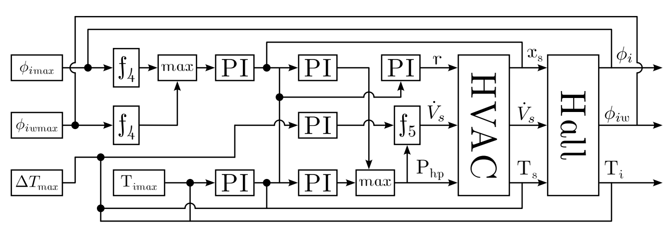


Fig. 5. Schematic of baseline control in summer mode

Figure 5), both the indoor RH ($\phi_i$ and $\phi_{iw}$) and the

indoor temperature $T_i$ are controlled in cascade with the specific humidity $q_s$ and the temperature $T_s$ of the supply air. The higher of the two control signals is used as both dehumidification and cooling are attained by increasing the heat pump's compressor power. The air fraction $r$ allows some balancing of the energy consumption, either towards more dehumidification or more cooling. The controller accomplishes this by seeking to drive both of the tracking errors of the inner cascade towards zero. Since the reduction of the two different tracking errors require $r$ to move in opposite directions the errors are not added but subtracted. The specific humidity error is converted to g/kg to achieve similar scale to the temperature error. In the case study, the minimum volumetric supply flow rate $\dot{V}_s$ was sufficient to keep the RH below its limits. Raising the flow rate for exchanging air with potentially drier outside air is not considered as a measure to reduce humidity in the summer mode control baseline. Instead, the volumetric supply flow $\dot{V}_s$ was increased when the heat pump was operating ($f_5$) and $T_i$ exceeded $T_s$ by more than 8 °C($\Delta T_{max}$). Limiting the temperature difference prevents uncomfortable droughts, but more importantly it can increase the cooling efficiency by increasing the COP and possibly reducing the amount of unnecessary dehumidification. The heating coil is not active in summer mode.
The HVAC mode is switched based on the 24-hour mean of the indoor temperature $T_i$ as well as the current $T_i$. If the 24-hour mean surpasses 23.5 °C or $T_i$ comes within 0.5 °C of $T_{imax}$, the HVAC is switched to summer mode. It switches back to winter mode, if the 24-hour mean falls below 19.5 °C or $T_i$ comes within 0.5 °C of $T_{imin}$.

2) Model predictive controller: The hall-HVAC system is highly nonlinear, especially with regard to the minimum energy consumption. At the lowest rate of 1200 m$^3$/h, the ventilation power consumption is 0.065 kW$_{\mathrm{el}}$, which increases to 3.506 kW$_{\mathrm{el}}$ at the highest rate of 6300 m$^3$/h. That is more than a magnitude difference in energy per air volume exchanged. This and other non-linearities are crucial in determining the energy optimal HVAC operation, so a non-linear MPC is employed. The MPC optimizes the sequence of the first four continuous manipulated variables $\dot{V}_s$, $r$, $\dot{Q}_h$ and $\dot{Q}_e$ for a given mode $m$ (see Table I). Adding the discrete mode variable $m$ would turn the problem from a nonlinear programming into a mixed-integer nonlinear programming problem, which is considerably harder to solve [21]. The optimal control problem can be described as

$$
\begin{aligned}
\min_{u_0,\ldots,u_{N-1}} \quad & \sum_{k=0}^{N-1} J_{ec}(k) + J_{\Delta}(k) + J_{vio}(k) \\
s.t. \quad & x_{k+1} = f(x_k, \hat{d}_k, u_k) \\
& y_k = h(x_k, \hat{d}_k, u_k) + v_{k0} \\
& s_k = g(y_k, r_k) \\
& u_{min} \leq u_k \leq u_{max} \\
& y_{min} \leq y_k \leq y_{max} \\
& x_0 = \hat{x_0}
\end{aligned}
\tag{13}
$$

where $N$ is the prediction and control horizon of $k$ time steps. $J_{ec}(k)$ is the energy cost, $J_{\Delta a}(k)$ the cost for actuator changes and $J_{vio}(k)$ holds the violations of the soft constraints at time step $k$. The manipulated variables $u_k$ are constrained as described in Table I. Of the outputs the heat pump power $P_{hp}$ is limited to a maximum of 5 kW$_{\mathrm{el}}$ and the temperature at the evaporator $T_{ev}$ is limited to a minimum of −20 °C to rule out nonphysical behavior of the heat pump. An additional optional constrain is to fall below the dew point at the evaporator ($T_{ev} < T_{dew}$). That is since above the dew point there is no gradient in the cost function for dehumidification. The simulated output $y_k$ is compensated by a constant bias over the prediction horizon, to eliminate the steady state error ($v_{k0} = y_{k-1} - \hat{y}_{k-1}$). As there are only measurements for $T_i$ and $\phi_i$, only these are corrected, all other assumed to be 0. The sampling time of the MPC is $T = 0.25$ h.

The energy cost is estimated in kWh using sampling time $T$ and the power of the heat pump (see Equation 4), fans (see Equation 5) and heat flow at the heating coil $\dot{Q}_h$, which is scaled with $\frac{1}{3}$ to account for the difference in gas and electricity prices:

$$J_{ec}(k) = (P_{hp}(k) + P_f(k) + \frac{1}{3}\dot{Q}_h(k))T \tag{14}$$

The change of an actuator $a$ is defined as $\Delta a(k) = a(k) - a(k-1)$. The actuators $a_j$ and corresponding weights $\gamma_j$ are displayed in Table II. Low weights are chosen here due to the low sample rate. Actuator change therefore only plays a minor role in the optimization. To calculate cost the weighted hourly rate of change is squared:

$$J_{\Delta}(k) = \sum_{j=1}^{4} (\gamma_j \Delta a_j(k) T^{-1})^2 \tag{15}$$

Four model outputs $y_j$ are soft constrained. Their limits

TABLE II
List of the actuators $a_j$ with change costs

| index | description | weight $\gamma$ |
|---|---|---|
| $a_1$ | $\dot{V}_s$ | 0.0450 |
| $a_2$ | $r$ | 0.0636 |
| $a_3$ | $\dot{Q}_h$ | 0.0021 |
| $a_4$ | $P_{hp}$ | 0.0125 |

and weights $\beta_j$ are displayed in Table III. The differences in weight $\beta_j$ are mainly due to scale. The slack variable $s_j$ is introduced, which is a measure for the violation of a limit of $y_j$:

$$J_{vio}(k) = \beta_4 s_4(k)^2 T + \sum_{j=1}^{3} \beta_j s_j(k+1)^2 T \tag{16}$$

with

$$y_{jmin} - s_j(k) \leq y_j(k) \leq y_{jmax} + s_j(k) \tag{17}$$
$$s_j \geq 0 \tag{18}$$

For optimization, the Sequential Quadratic Programming Algorithm is used like described in [22]. Since the operating mode $m$ is not part of the optimization, an optimal operation over the prediction horizon is only known for a constant mode. So both optimizations are performed separately. In winter mode a single optimization is performed. In summer mode optimization is carried out just the same. However, in the case that humidity soft constraints of $\phi_i$ and $\phi_{iw}$ are violated, the solution can remain in a local optimum, where cooling the air increases energy costs, while not reducing the soft constraint violation, since the dew point at $T_{ev}$ is not reached and thus the air not dehumidified. When that case occurs, two additional optimizations are carried out, to potentially find a more optimal solution. In the first additional optimization in every time step $k$ the temperature at the evaporator $T_{ev}$ is constrained below its dew point ($T_{ev}(k) < T_{dew}$), where the humidity soft constraints got within 2 % of their boundary in $k+1$. The second additional optimization is again performed without the additional constraint, but with the solution of the previous optimization as an initial sequence. Of the different solutions in summer mode and winter mode, the solution with lowest cost is selected.

TABLE III
List of the model outputs $y_j$ with soft constraints

| index | description | min | max | weight $\beta$ |
|---|---|---|---|---|
| $y_1$ | $T_i$ | 12 °C/17 °C | 26 °C | 1 |
| $y_2$ | $\phi_i$ | - | 70 % | 5 |
| $y_3$ | $\phi_{iw}$ | - | 90 % | 5 |
| $y_4$ | $T_s$ | 3 °C | 30 °C | 1 |

### D. Experiment

The MPC and baseline controller are evaluated in a model-in-the-loop study covering 04-03-2022 to 03-03-2023 (Central European Summer Time). Roof-mounted weather data provide disturbances, while building parameters are identified via nonlinear least-squares. In addition, some building parameters are considered variable and were also estimated in advance by an EKF with measured data and a model of a current HVAC unit [15] that is replaced in the model-in-the-loop setting with a model of the future unit. The simulation runs with a sample time of 1 min and the MPC has a sample time of 15 min. Both models are nearly identical, except that the MPC incorporates two neural nets for condensation handling to accelerate computation. Additional mismatch between the models occurs due to different sample rates and the change of building model parameters. The MPC assumes the model parameters to remain constant over the prediction horizon. To address the very small model mismatch, we integrate an artificial mismatch, where we changed the model parameters of the internal hall model by 10 % compared to the simulation model. The root mean square error of the internal model results in a mismatch of 0.34 °C for indoor temperature and 0.89 % for indoor humidity for a prediction of 1 h ahead and for 24 h 0.88 °C and 2.92 % which is large compared to the fit of the experimental model. Currently, no weather forecast data are used, but disturbances over the prediction horizon are assumed to be known. Three different factors are investigated in the comparison of the MPC with our baseline controller:

1) The prediction/control horizon.
2) How the mode is switched: Either by the same rules as the baseline control or the more cost optimal.
3) How can the cost optimal switching MPC handle additional model mismatch by changing the hall parameters of the internal MPC model by 10 % .

As an evaluation metric, the MPC cost function is used. Since it is tuned for a sample time of 15 min, the simulation results are averaged over the MPC sample windows.

To include higher prediction horizons in an adequate simulation time and to be able to run this MPC on the dedicated hardware in real time, blocking is introduced for prediction horizon of 24 h or 96 time steps. This limits the flexibility of the MPC in later time steps, since the manipulated variables can then only be adjusted uniformly for the entire block [23]. The 96 time steps are separated into 15 blocks. The first 4 have a sample time of 15 min the next 2 have 30 min then 2 with 1 h, 2 with 2 h and 4 with 4 h sample time.

## III. Results & Discussion

Figure 6 shows the operational costs over the whole year that are computed according to the MPC cost function. The costs are displayed for the non predictive baseline control and the three different MPC simulations, where the mode is switched according to the same rules as in the baseline (MPC1), according to the cost of the two different modes over the prediction horizon (MPC2) and a model parameter mismatch of the hall of 10 % added to MPC2 (MPC2-m). In this evaluation, we exclude the violation of the humidity on the wall as we do not have a sensor and therefore cannot feed back the disturbance in the real system, so an MPC with a model mismatch cannot correct its measurements. The annual cost in $\text{kWh}_{\text{el}}$ or equivalents is relatively low, which is due to the size of the facility and the broad temperature boundaries. Four components dominate the annual cost, which are the energy consumption of the fans $E_f$, of the heat pump $E_{hp}$, the heating coil $E_{hc}$ and the violations of the soft constraints of the indoor temperature $T_{ivio}$. The other parts of the cost are summarized as others.

With an increasing control and prediction horizon in MPC1, MPC2 and MPC2-m, the improvements in cost

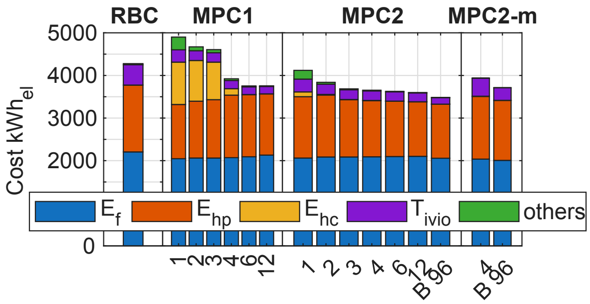


Fig. 6. Cost in kWh$_{\mathrm{el}}$ of operation over the period of one year for the baseline controller, the two different MPCs and a MPC with model mismatch. For the MPCs cost is given for a control and prediction horizon of 1 (15 min) to 96 steps (24 *h*).

quickly decrease. The first improvements at low prediction horizons are due to the high air exchange rate of the HVAC unit (i.e. low time constant), which is a strong contributor to the indoor climate and currently holds all of the manipulated variables. Further improvements are possible if the prediction horizon is selected quite large, such as 96 time steps which correspond to 24 h. The improvements with bigger prediction horizons are due to the increase in planning capability, including future weather and setpoints, as well as the ability to address the thermal capacities of the building. Adding model mismatch in MPC2-m results in a higher cost compared to MPC2. Looking at the cost reduction of the MPC compared to the base controller, we find the following improvements:

- MPC1 (prediction horizon of 12): 12.1 %
- MPC2 (prediction horizon of 12): 15.8 %
- MPC2 (blocked prediction horizon of 96): 18.5 %
- MPC2-m (blocked prediction horizon of 96): 13.1 %

In Figure 7 the average costs are plotted over the year. We can observe that during the transition months in October and November 2022 MPC2-12 and MPC2-m 96B have a cost advantage over the base and MPC1 controller. The lower part of Figure 7 shows that controller MPC2-12 switches during summertime between winter and summer mode (winter = true), while MPC1 and base controller remain in summer mode. This more optimal switching of MPC2 reduces overall costs. Interestingly, MPC1 uses the heating coil (Figure 7), which is not the case in the baseline or at higher prediction horizons. In Figure 8 (summer day) it can be observed that MPC1-4 uses the heating coil to increase the temperature and, therefore, reduces the relative humidity. This might be cheaper in the prediction horizon of 1 hour, but in the long range it results in a temperature rise, and therefore it has to cool later on. Instead, MPC1-12 can calculate the advantage of using the heat pump to cool and condensate the air, resulting in lower costs in total. The base controller instead is programmed to use the heat pump in summer mode to dry. However, it is clear that MPC1-12 uses less energy compared to the base. Looking

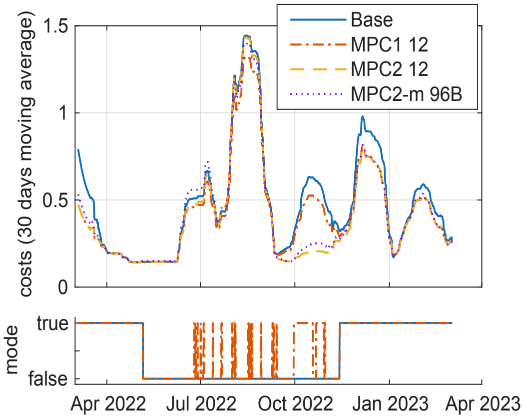


Fig. 7. Average cost of 30 days and mode (true: winter / false: summer) plotted over the examplary period for different controllers.

at the end of the day when the temperature reaches a maximum of 26 °C, all controllers use the heat pump to cool. In contrast to the base, the MPC starts early with the cooling and uses the flaps as well to increase the airflow. This decreases the amount of cooling energy by the heat pump.

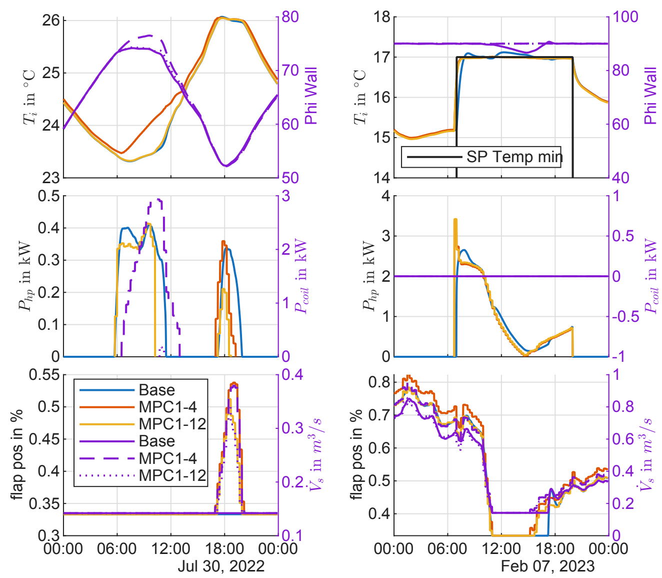


Fig. 8. Temperature and relative humidity in the hall and corresponding control variables of the base controller compared to MPC1 with 4 and 12 steps prediction and control horizon. On the left side a typical summer day and on the right side a typical winter day in corresponding modes of the controller.

Looking at the average moving energy costs over the year Figure 7, it is clear that the MPC outperforms the Base controller, especially during the coldest time of the year. On the left side of Figure 8 you find a typical winter day, where you can observe that the MPC can keep the temperature to the lower limit during work time. The base control cannot plan the temperature rise at 6:15 o'clock and therefore violates the temperature limit at the beginning. In general, all controllers use similar control variables to keep the temperature and relative humidity, and also the MPC can keep the boundaries a bit better.

## IV. Conclusion & Outlook

In this paper, we could show that a nonlinear MPC which directly controls the components of the HVAC system can outperform an advanced base controller in a realistic framework of an RAS. The MPC achieves temperature and humidity in the range with minimal energy consumption. We addressed the missing gradient for de-humidification. We could show that the more optimal switching between the winter mode and the summer mode of the controller increases the savings as well as longer prediction and control horizons. We also investigated the influence of model mismatch and could show that an artificial model mismatch larger than the observed mismatch in the MPC model still results in savings of around 13 % to the base controller in the selected cost function. Due to the realistic test environment, we are confident that the controller performance will match the simulation results as soon as it is implemented in the RAS. For an implementation, the minimal power of the heat pump and heating coil as well as a state switch off have to be included. For a better performance of the model mismatch case it would be advantageous to estimate the deviation by the Kalman Filter, which is used to estimate the model parameter and the model state.

## Declaration of Competing Interest

## Acknowledgement

The authors gratefully acknowledge the financial support by the "Landesprogramm Fischerei und Aquakultur" with funds provided by the European Union, the European Maritime, Fisheries and Aquaculture Fund (EMFAF), the federal government, as well as the federal state Schleswig-Holstein (Grant number: SH-2.1.7-001) and the "Gesellschaft für Energie und Klimaschutz Schleswig-Holstein" EKSH.

## References

[1] M. González-Torres, L. Pérez-Lombard, J. F. Coronel, I. R. Maestre, and D. Yan, "A review on buildings energy information: Trends, end-uses, fuels and drivers," Energy Reports, vol. 8, pp. 626–637, 2022.

[2] L. Pérez-Lombard, J. Ortiz, and C. Pout, "A review on buildings energy consumption information," Energy and Buildings, vol. 40, pp. 394–398, 01 2008.

[3] Council of European Union, "Directive (eu) 2024/1275 of the european parliament and of the council on the energy performance of buildings," Official Journal of the European Union, vol. L 2024/1275, pp. 1–68, 24.4.2024.

[4] J. Drgoňa, J. Arroyo, I. Cupeiro, D. Blum, K. Arendt, D. Kim, E. Olle, J. Oravec, M. Wetter, D. Vrabie, and L. Helsen, "All you need to know about model predictive control for buildings," Annual Reviews in Control, vol. 50, 10 2020.

[5] G. Serale, M. Fiorentini, A. Capozzoli, D. Bernardini, and A. Bemporad, "Model predictive control (mpc) for enhancing building and hvac system energy efficiency: Problem formulation, applications and opportunities," Energies, vol. 11, p. 631, 03 2018.

[6] L. Jingyun and L. Ping, "Temperature and humidity control with a model predictive control method in the air-conditioning system," in 2017 International Conference on Advanced Mechatronic Systems (ICAMechS), 2017, pp. 408–412.

[7] W.-H. Chen and F. You, "An energy optimization model for commercial buildings with renewable energy systems via nonlinear mpc," Chemical Engineering Transactions, vol. 94, pp. 505–510, Sep. 2022.

[8] P. Bahramnia, S. M. Hosseini Rostami, J. Wang, and G.-j. Kim, "Modeling and controlling of temperature and humidity in building heating, ventilating, and air conditioning system using model predictive control," Energies, vol. 12, pp. 1–24, 12 2019.

[9] N. S. Raman, K. Devaprasad, and P. Barooah, "Mpc-based building climate controller incorporating humidity," in 2019 American Control Conference (ACC), 2019, pp. 253–260.

[10] S. Yang, M. P. Wan, B. F. Ng, T. Zhang, S. Babu, Z. Zhang, W. Chen, and S. Dubey, "A state-space thermal model incorporating humidity and thermal comfort for model predictive control in buildings," Energy and Buildings, vol. 170, pp. 25–39, 2018.

[11] J. Goo, Y. Kwak, J. Kim, J. Kang, H. Shin, S.-K. Jo, and J.-H. Huh, "Development of early design tool for aquaculture buildings using building performance simulation: A case study of an indoor fish farm," Developments in the Built Environment, vol. 17, p. 100363, 2024.

[12] S. Fux, A. Ashouri, M. Benz, and L. Guzzella, "Ekf based self-adaptive thermal model for a passive house," Energy and Buildings, pp. –, 01 2012.

[13] M. Maasoumy, M. Razmara, M. Shahbakhti, and A. Vincentelli, "Handling model uncertainty in model predictive control for energy efficient buildings," Energy and Buildings, vol. 77, p. 377–392, 07 2014.

[14] G. Gehlert, M. Griese, M. Schlachter, and C. Schulz, "Analysis and optimisation of dynamic facility ventilation in recirculation aquacultural systems," Aquacultural Engineering, vol. 80, pp. 1–10, 2018.

[15] J. Klinge, D. Wekerle, and K. Völtzer, "Mpc-suitable hygrothermal, data-based modeling of an aquaculture hall for the (energetic) optimisation of inner climate," in 2023 European Control Conference (ECC). IEEE, 2023, pp. 1–8.

[16] WMO, "Guide to instruments and methods of observation, volume i: Measurement of meteorological variables (8th ed.)," World Meteorological Organization Geneva, 2021.

[17] D. Sonntag, "Advancements in the field of hygrometry," Meteorologische Zeitschrift, pp. 51–66, 1994.

[18] O. Ruhnau, L. Hirth, and A. Praktiknjo, "Time series of heat demand and heat pump efficiency for energy system modeling," Scientific data, vol. 6, no. 1, p. 189, 2019.

[19] J. Drgoňa, J. Arroyo, I. C. Figueroa, D. Blum, K. Arendt, D. Kim, E. P. Ollé, J. Oravec, M. Wetter, D. L. Vrabie, et al., "All you need to know about model predictive control for buildings," Annual Reviews in Control, vol. 50, pp. 190–232, 2020.

[20] BAuA, 2010, technische Regel für Arbeitsstätten ASR A3.5 Raumtemperatur, Gemeinsames Ministerialblatt (GMBl), Ausgabe Juni 2010. (p. 751).

[21] K. Deng, Y. Sun, S. Li, Y. Lu, J. Brouwer, P. G. Mehta, M. Zhou, and A. Chakraborty, "Model predictive control of central chiller plant with thermal energy storage via dynamic programming and mixed-integer linear programming," IEEE Transactions on Automation Science and Engineering, vol. 12, no. 2, pp. 565–579, 2015.

[22] J. Nocedal and S. Wright, Numerical optimization, 2nd ed., ser. Springer series in operations research. New York, NY: Springer, 2006.

[23] R. C. Shekhar and C. Manzie, "Optimal move blocking strategies for model predictive control," Automatica, vol. 61, p. 27–34, 2015.